



HAL
open science

A simple pseudospectral method for the computation of the time-dependent Dirac equation with Perfectly Matched Layers. Application to quantum relativistic laser physics

X Antoine, E Lorin

► **To cite this version:**

X Antoine, E Lorin. A simple pseudospectral method for the computation of the time-dependent Dirac equation with Perfectly Matched Layers. Application to quantum relativistic laser physics. 2018. hal-01929065

HAL Id: hal-01929065

<https://hal.science/hal-01929065>

Preprint submitted on 20 Nov 2018

HAL is a multi-disciplinary open access archive for the deposit and dissemination of scientific research documents, whether they are published or not. The documents may come from teaching and research institutions in France or abroad, or from public or private research centers.

L'archive ouverte pluridisciplinaire **HAL**, est destinée au dépôt et à la diffusion de documents scientifiques de niveau recherche, publiés ou non, émanant des établissements d'enseignement et de recherche français ou étrangers, des laboratoires publics ou privés.

A simple pseudospectral method for the computation of the time-dependent Dirac equation with Perfectly Matched Layers. Application to quantum relativistic laser physics.

X. Antoine^a, E. Lorin^{b,c}

^a*Institut Elie Cartan de Lorraine, Université de Lorraine, Sphinx team, Inria Nancy-Grand Est, F-54506 Vandoeuvre-lès-Nancy Cedex, France*

^b*School of Mathematics and Statistics, Carleton University, Ottawa, Canada, K1S 5B6*

^c*Centre de Recherches Mathématiques, Université de Montréal, Montréal, Canada, H3T 1J4*

Abstract

A simple time-splitting pseudospectral method for the computation of the Dirac equation with Perfectly Matched Layers (PML) is proposed. Within this approach, basic and widely used FFT-based solvers can be adapted without much effort to compute Initial Boundary Value Problems (IBVP) for the time-dependent Dirac equation with absorbing boundary layers. Some numerical examples from laser-physics are proposed to illustrate the method.

Keywords: Dirac equation; time-splitting; pseudospectral approximation; Perfectly Matched Layers; high-order accuracy

1. Introduction

This paper is concerned with the numerical computation of the time-dependent Dirac equation, especially for physical problems involving delocalized wavefunctions. More specifically, we are interested in the numerical solution to the Dirac equation on a truncated domain with absorbing boundary layers, hence limiting the periodic conditions effects. In this goal, we then propose a simple combination of a pseudospectral method with Perfectly Matched Layers (PMLs), allowing to consider delocalized wavefunctions, as for instance observed when quantum relativistic particles are subject to strong fields. Thanks to a relatively new and simple Fourier-based discretization of spatial differential operators, it is possible to impose PML for solving the Dirac equation on a bounded domain. Although, overall, the Fourier-based method still imposes periodic boundary conditions, the outgoing/incoming waves are in fact mainly absorbed. We think that due to the simplicity of the proposed method, most of existing Fourier-based codes could easily be modified to include the proposed methodology. The Dirac equation is a relativistic wave equation which has gain much attention these past 15 years due to the development of 2-d material, such as

Email addresses: xavier.antoine@univ-lorraine.fr (X. Antoine), elorin@math.carleton.ca (E. Lorin)

graphene [20, 21, 37], intense-laser-molecule interaction [18, 30, 40, 45], in particular for pair production [25], or from heavy ion collisions modeling and simulation for quark-antiquark production [29, 44, 50]. In the same time, there has been a tremendous progress in the development of efficient and accurate computational methods for the solution to the Dirac equation [4, 9, 10, 11, 14, 22, 23, 26, 27, 31, 39, 40, 46], modeling in particular molecules subject to intense external laser fields. In this spirit, we have developed [25], a Schwinger-like pair production procedure from the interaction of intense laser fields with heavy molecules occurring at specific resonances [25, 24].

In this paper, we are more specifically interested in the interaction of relativistic interaction of atoms, molecules or wavepackets with intense and short laser pulses. The key point is that the laser field actually delocalizes the wavefunction, and the latter can actually interact with the domain boundary. In order to avoid artificial reflection it is necessary to impose absorbing boundary conditions [5], absorbing complex potentials or perfectly matched layers [43]. Theoretically, this approach allows to benefit from the spectral convergence and simplicity of Fourier-based methods, more specifically pseudospectral, on bounded domains reducing the periodic boundary condition effect thanks to artificial wave absorption at the domain boundary. Perfectly Matched Layers are now widely used in many engineering and physics simulations codes [1, 12, 13, 15, 16, 17, 19, 34, 35, 42, 48, 49, 51, 52] to model exterior domains and to avoid any unphysical reflection at the boundary. PML for the Dirac equation were developed in [43] and approximated with a real space method. The derivation of high-order ABCs for the Dirac equation were proposed in [5]. We also refer to [6] for an overview of PMLs and ABCs for quantum wave equations including the Dirac equation and to [4, 7, 8, 9, 11, 14, 22, 26, 28, 32, 33, 38, 39, 41] for different approaches for solving the Dirac equation in real or Fourier space.

The combination of pseudospectral methods and PMLs is possible thanks to the following simple and original idea. For example in the x -direction, let us denote by ξ_x the dual Fourier variable and by \mathcal{F}_x (resp. \mathcal{F}_x^{-1}) the Fourier (resp. inverse Fourier) transform in x . We consider a as a given x -dependent function. Then, for any function f , it is possible to formally rewrite $a(x)\partial_x f(x)$ as $\mathcal{F}_x^{-1}(a(x)\mathbf{i}\xi_x\mathcal{F}(f)(\xi_x))(x)$ on an unbounded domain (pseudodifferential operator representation [47]). Let us remark that the latter is a real space function, although the derivative is approximated using the Fourier transform, and the function $(x, \xi_x) \mapsto \mathbf{i}a(x)\xi_x$ is nothing but the symbol of $a(x)\partial_x$. In practice the function a involves the stretching coordinates function modeling the PML on a bounded domain allowing real space non-reflecting conditions at the domain boundary.

The time-dependent Dirac equation under consideration reads [36]

$$\mathbf{i}\partial_t\psi(t, \mathbf{x}) = H\psi(t, \mathbf{x}), \quad (1)$$

where $\psi(t, \mathbf{x})$ is the time and coordinate dependent four-spinor, and H is the Hamiltonian operator. The latter is given by

$$H = \boldsymbol{\alpha} \cdot [c\mathbf{p} - e\mathbf{A}(t, \mathbf{x})] + \beta mc^2 + \mathbb{I}_4 V(t, \mathbf{x}), \quad (2)$$

where the momentum operator is $\mathbf{p} = -\mathbf{i}\nabla$. More specifically, the Dirac equation that we

consider reads [36]

$$\begin{aligned} \mathbf{i}\partial_t\psi(t, \mathbf{x}) = & \left\{ \alpha_x \left[-\mathbf{i}c\partial_x - eA_x(t, \mathbf{x}) \right] + \alpha_y \left[-\mathbf{i}c\partial_y - eA_y(t, \mathbf{x}) \right] \right. \\ & \left. + \alpha_z \left[-\mathbf{i}c\partial_z - eA_z(t, \mathbf{x}) \right] + \beta mc^2 + \mathbb{I}_4 V(t, \mathbf{x}) \right\} \psi(t, \mathbf{x}), \end{aligned} \quad (3)$$

where $\psi(t, \mathbf{x}) \in L^2(\mathbb{R}^3) \otimes \mathbb{C}^4$ is the time and coordinate ($\mathbf{x} = (x, y, z)$) dependent four-spinor. In (3), $\mathbf{A}(t, \mathbf{x})$ represents the three space components of the electromagnetic vector potential, $V(t, \mathbf{x}) = eA_0(t, \mathbf{x}) + V_{\text{nuc.}}(\mathbf{x})$ is the sum of the scalar and interaction potentials, e is the electric charge (with $e = -|e|$ for an electron), \mathbb{I}_4 is the 4×4 unit matrix and $\boldsymbol{\alpha} = (\alpha_\nu)_{\nu=1, \dots, 4}, \beta$ are the Dirac matrices. In this work, the Dirac representation is used, where

$$\alpha_\nu = \begin{bmatrix} 0 & \sigma_\nu \\ \sigma_\nu & 0 \end{bmatrix}, \quad \beta = \begin{bmatrix} \mathbb{I}_2 & 0 \\ 0 & -\mathbb{I}_2 \end{bmatrix}. \quad (4)$$

The σ_ν are the usual 2×2 Pauli matrices defined as

$$\sigma_x = \begin{bmatrix} 0 & 1 \\ 1 & 0 \end{bmatrix}, \quad \sigma_y = \begin{bmatrix} 0 & -\mathbf{i} \\ \mathbf{i} & 0 \end{bmatrix} \quad \text{and} \quad \sigma_z = \begin{bmatrix} 1 & 0 \\ 0 & -1 \end{bmatrix}, \quad (5)$$

while \mathbb{I}_2 is the 2×2 unit matrix. Note that the light velocity c and fermion mass m are kept explicit in Eq. (2), allowing to adapt the method easily to natural or atomic units (a.u.).

The paper is organized as follows. We recall the basics of PMLs for the Dirac equation in Section 2. Section 3 is dedicated to the derivation of the pseudospectral approximation for the Initial Boundary Value Problem (IBVP) time-dependent Dirac equation on a bounded domain with PML. Numerical experiments are presented in Section 4. We finally conclude in Section 5.

2. PML for the Dirac equation

The time-dependent Dirac equation is then considered on a bounded (truncated) physical domain denoted by \mathcal{D}_{Phy} . We add a layer, that is called \mathcal{D}_{PML} , surrounding \mathcal{D}_{Phy} , and stretch the coordinates in all the directions. The overall computational domain is next defined by: $\mathcal{D} = \overline{\mathcal{D}_{\text{Phy}} \cup \mathcal{D}_{\text{PML}}}$. We refer to [6] for the construction of PMLs for quantum wave equations and more specifically to [43] for the derivation and analysis of PMLs for the Dirac equation.

The starting point is the stretching of the real coordinates in the complex plane. In [43], the author uses the following variables

$$\tilde{\nu} = \nu + \frac{\mathbf{i}}{\omega} \int_{L_\nu^*}^\nu \sigma(s) ds,$$

where ω is the dual Fourier variable to t and the so-called *absorbing function* σ is such that $\sigma(\nu) = 0$ if $s < L_\nu^*$. Then, the partial derivative ∂_ν , with $\nu = x, y, z$, is shown to be formally

transformed into

$$\partial_\nu \psi(t, \cdot) \rightarrow \frac{\partial_t}{\partial_t + \tilde{\sigma}_\nu(\nu)} \partial_\nu \psi(t, \cdot) = \frac{1}{2\pi} \int_{\mathbb{R}} \frac{\omega e^{i\omega t}}{\omega - i\tilde{\sigma}_\nu(\nu)} \partial_\nu \mathcal{F}_t \psi(\omega, \cdot) d\omega, \quad (6)$$

where \mathcal{F}_t (resp. \mathcal{F}_ν) denotes the Fourier transform with respect to t (resp. ν) and

$$\tilde{\sigma}_\nu(\nu) = \begin{cases} \sigma(|\nu| - L_\nu), & L_\nu^* \leq |\nu| < L_\nu, \\ 0, & |\nu| < L_\nu^*. \end{cases}$$

Let us remark that the transformation (6) can also be formally rewritten as

$$\partial_\nu \psi(t, \cdot) \rightarrow \frac{1}{1 + \tilde{\sigma}_\nu(\nu) \partial_t^{-1}} \partial_\nu \psi(t, \cdot).$$

In the following, we will rather consider the following change of variables [52] involving only the space variable

$$\tilde{\nu} = \nu + e^{i\theta} \int_{L_\nu^*}^{\nu} \sigma(s) ds,$$

where $\theta \in (0, \pi/2)$. We then define

$$S_\nu(\nu) := 1 + e^{i\theta\nu} \tilde{\sigma}(\nu),$$

with $\nu = x, y, z$. In the following, the partial derivatives are transformed into

$$\partial_\nu \rightarrow \frac{1}{S_\nu(\nu)} \partial_\nu = \frac{1}{1 + e^{i\theta\nu} \tilde{\sigma}_\nu(\nu)} \partial_\nu, \quad (7)$$

where $\tilde{\sigma}$ vanishes in \mathcal{D}_{Phy} and S_ν is equal to 1. From now on, let us consider the transformation (7), and the associated new Hamiltonian

$$H_{\text{PML}} = \boldsymbol{\alpha} \cdot [c\mathbf{T} \cdot \mathbf{p} - e\mathbf{A}(t, \mathbf{x})] + \beta mc^2 + \mathbb{I}_4 V(t, \mathbf{x}), \quad (8)$$

where $\mathbf{T} = (S_x^{-1}(x), S_y^{-1}(y), S_z^{-1}(z))^T$. Several types of functions can be selected. An exhaustive study of the absorbing functions σ is proposed in [3] for Schrödinger equations

$$\text{Type I: } \sigma_0(\nu + \delta_\nu)^2, \quad \text{Type II: } \sigma_0(\nu + \delta_\nu)^3, \quad \text{Type III: } -\sigma_0/\nu,$$

$$\text{Type IV: } \sigma_0/\nu^2, \quad \text{Type V: } -\sigma_0/\nu - \sigma_0/\delta_\nu, \quad \text{Type VI: } \sigma_0/\nu^2 - \sigma_0/\delta_\nu^2,$$

for $\nu = x, y, z$. The main difficulty from the pseudospectral point of view is the space-dependence of the coefficients S_ν^{-1} which prevents the direct application of the Fourier transform on the equation. A simple trick will however allow for combining the efficiency of the pseudospectral method and the computation of the non-constant coefficient Dirac equation.

3. Pseudospectral-PML (PS-PML) method

A splitting of the Dirac Hamiltonian is used below. Although operator splitting is not fundamentally required in the proposed methodology, it allows to simplify the implementation of the method while keeping a good accuracy. Based on (2), we define the operators

$$A = -icS_x^{-1}(x)\alpha_x\partial_x, \quad (9)$$

$$B = -icS_y^{-1}(y)\alpha_y\partial_y, \quad (10)$$

$$C = -icS_z^{-1}(z)\alpha_z\partial_z, \quad (11)$$

$$D = \beta mc^2 + \mathbb{I}_4 V(t, \mathbf{x}) - e\boldsymbol{\alpha} \cdot \mathbf{A}(t, \mathbf{x}). \quad (12)$$

From time t_n to t_{n+1} , we then successively solve [39] (the \mathbf{x} -dependence in the wavefunction argument for notational convenience)

$$i\partial_t\psi^{(1)}(t) = A\psi^{(1)}(t), \quad \psi^{(1)}(t_n) = \psi^n, \quad t \in [t_n, t_{n_1}] \quad (13)$$

$$i\partial_t\psi^{(2)}(t) = B\psi^{(2)}(t), \quad \psi^{(2)}(t_n) = \psi^{(1)}(t_{n_1}), \quad t \in [t_n, t_{n_2}] \quad (14)$$

$$i\partial_t\psi^{(3)}(t) = C\psi^{(3)}(t), \quad \psi^{(3)}(t_n) = \psi^{(2)}(t_{n_2}), \quad t \in [t_n, t_{n_3}] \quad (15)$$

$$i\partial_t\psi^{(4)}(t) = D\psi^{(4)}(t), \quad \psi^{(4)}(t_n) = \psi^{(3)}(t_{n_3}), \quad t \in [t_n, t_{n+1}] \quad (16)$$

$$\text{and } \psi^{n+1} = \psi^{(4)}(t_{n+1}), \quad (17)$$

where $t_{n_i} - t_n = \Delta t$ for $i \in \{1, \dots, 3\}$. In the next subsections, we detail the space-time approximation of equations (13)-(16). Cylindrical coordinates could be used as well (see e.g. [26]).

3.1. Pseudospectral approximation in space

We consider for convenience the 3-dimensional system in cartesian coordinates, for $\nu = x, y, z$ in the domain $\mathcal{D} = [-a_x, a_x] \times [-a_y, a_y] \times [-a_z, a_z]$,

$$i\partial_t\psi(t) = -ic\alpha_\nu S_\nu^{-1}(\nu)\partial_\nu\psi(t), \quad \psi(t_n) = \psi^n, \quad t \in [t_n, t_{n+1}]$$

and we use the same notation as in [2]. We first diagonalize $\alpha_\nu = \Pi_\nu D_\nu \Pi_\nu^T$, where

$$D_\nu = \begin{pmatrix} 1 & 0 & 0 & 0 \\ 0 & 1 & 0 & 0 \\ 0 & 0 & -1 & 0 \\ 0 & 0 & 0 & -1 \end{pmatrix}.$$

The matrices Π_ν are defined as follows

$$\begin{aligned}\Pi_x &= \frac{1}{\sqrt{2}} \begin{pmatrix} 0 & 1 & 1 & 0 \\ 1 & 0 & 0 & -1 \\ 1 & 0 & 0 & 1 \\ 0 & 1 & -1 & 0 \end{pmatrix}, \\ \Pi_y &= \frac{1}{\sqrt{2}} \begin{pmatrix} 0 & -i & -i & 0 \\ 1 & 0 & 0 & 1 \\ -i & 0 & 0 & i \\ 0 & 1 & -1 & 0 \end{pmatrix}, \\ \Pi_z &= \frac{1}{\sqrt{2}} \begin{pmatrix} 1 & 0 & 0 & -1 \\ 0 & -1 & -1 & 0 \\ 1 & 0 & 0 & 1 \\ 0 & 1 & -1 & 0 \end{pmatrix}.\end{aligned}$$

We set $\phi := \Pi_\nu^T \psi$, which then satisfies

$$i\partial_t \phi(t) = -icD_\nu S_\nu^{-1}(\nu)\partial_\nu \phi(t), \quad \phi(t_n) = \Pi_\nu^T \psi^n, \quad t \in [t_n, t_{n+1}).$$

We denote the set of grid-points by

$$\mathcal{D}_{N_x, N_y, N_z} = \left\{ \mathbf{x}_{k_1, k_2, k_3} = (x_{k_1}, y_{k_2}, z_{k_3}) \right\}_{(k_1, k_2, k_3) \in \mathcal{O}_{N_x N_y N_z}}$$

with

$$\mathcal{O}_{N_x N_y N_z} = \{(k_1, k_2, k_3) \in \mathbb{N}^3 / k_1 = 0, \dots, N_x - 1; k_2 = 0, \dots, N_y - 1; k_3 = 0, \dots, N_z - 1\}.$$

Then, let us introduce the following mesh sizes

$$\begin{aligned}x_{k_1+1} - x_{k_1} &= h_x = 2a_x/N_x, \\ y_{k_2+1} - y_{k_2} &= h_y = 2a_y/N_y, \\ z_{k_3+1} - z_{k_3} &= h_z = 2a_z/N_z.\end{aligned}\tag{18}$$

The corresponding discrete wavenumbers are defined by $\boldsymbol{\xi} := (\xi_p, \xi_q, \xi_r)$, where $\xi_p = p\pi/a_x$ with $p \in \{-N_x/2, \dots, N_x/2 - 1\}$, $\xi_q = q\pi/a_y$ with $q \in \{-N_y/2, \dots, N_y/2 - 1\}$ and $\xi_r = r\pi/a_z$ with $r \in \{-N_z/2, \dots, N_z/2 - 1\}$. In the sequel of the paper, we denote by $\phi^{(\ell)}$, with $\ell \in \{1, 2, 3, 4\}$, the ℓ th component of the spectral approximation of $\phi = \Pi_\nu^T \psi$, with $\nu = x, y, z$. We also use the notation $\phi_{k_1}^{(\ell)}(t, y, z) = \phi^{(\ell)}(t, x_{k_1}, y, z)$, $\phi_{k_2}^{(\ell)}(t, x, z) = \phi^{(\ell)}(t, x, y_{k_2}, z)$ and $\phi_{k_3}^{(\ell)}(t, x, y) = \tilde{\phi}^{(\ell)}(t, x, y, z_{k_3})$. The partial Fourier coefficients are such that

$$\left\{ \begin{aligned}\widehat{\phi}_p^{(\ell)}(t, y, z) &= \sum_{\substack{k_1=0 \\ N_y-1}}^{N_x-1} \phi_{k_1}^{(\ell)}(t, y, z) e^{-i\xi_p(x_{k_1}+a_x)}, \\ \widehat{\phi}_q^{(\ell)}(t, x, z) &= \sum_{\substack{k_2=0 \\ N_z-1}}^{N_y-1} \phi_{k_2}^{(\ell)}(t, x, z) e^{-i\xi_q(y_{k_2}+a_y)}, \\ \widehat{\phi}_r^{(\ell)}(t, x, y) &= \sum_{k_3=0}^{N_z-1} \phi_{k_3}^{(\ell)}(t, x, y) e^{-i\xi_r(z_{k_3}+a_z)}.\end{aligned}\right.$$

We can then introduce the inverse partial Fourier pseudospectral approximations, in the x -, y - and z -directions, respectively,

$$\left\{ \begin{array}{l} \tilde{\phi}_{k_1}^{(\ell)}(t, y, z) = \frac{1}{N_x} \sum_{p=-N_x/2}^{N_x/2-1} \widehat{\phi}_p^{(\ell)}(t, y, z) e^{i\xi_p(x_{k_1}+a_x)}, \\ \tilde{\phi}_{k_2}^{(\ell)}(t, x, z) = \frac{1}{N_y} \sum_{q=-N_y/2}^{N_y/2-1} \widehat{\phi}_q^{(\ell)}(t, x, z) e^{i\xi_q(y_{k_2}+a_y)}, \\ \tilde{\phi}_{k_3}^{(\ell)}(t, x, y) = \frac{1}{N_z} \sum_{r=-N_z/2}^{N_z/2-1} \widehat{\phi}_r^{(\ell)}(t, x, y) e^{i\xi_r(z_{k_3}+a_z)}. \end{array} \right.$$

We finally define the approximate first-order partial derivatives by

$$\left\{ \begin{array}{l} \partial_x \phi^{(\ell)}(t_n, \mathbf{x}_{k_1, k_2, k_3}) \approx \{[[\partial_x]]\phi^{(\ell)}\}_{k_1, k_2, k_3} := \frac{1}{N_x} \sum_{p=-N_x/2}^{N_x/2-1} i\xi_p (\widehat{\phi}_{k_2, k_3}^{(\ell)})_p e^{i\xi_p(x_{k_1}+a_x)}, \\ \partial_y \phi^{(\ell)}(t_n, \mathbf{x}_{k_1, k_2, k_3}) \approx \{[[\partial_y]]\phi^{(\ell)}\}_{k_1, k_2, k_3} := \frac{1}{N_y} \sum_{q=-N_y/2}^{N_y/2-1} i\xi_q (\widehat{\phi}_{k_1, k_3}^{(\ell)})_q e^{i\xi_q(y_{k_2}+a_y)}, \\ \partial_z \phi^{(\ell)}(t_n, \mathbf{x}_{k_1, k_2, k_3}) \approx \{[[\partial_z]]\phi^{(\ell)}\}_{k_1, k_2, k_3} := \frac{1}{N_z} \sum_{r=-N_z/2}^{N_z/2-1} i\xi_r (\widehat{\phi}_{k_1, k_2}^{(\ell)})_r e^{i\xi_r(z_{k_3}+a_z)}. \end{array} \right. \quad (19)$$

In the following, the index h will be used (e.g. in $\phi_h^n = \{\phi_{k_1, k_2, k_3}^n\}_{k_1, k_2, k_3}$) to denote a spectral approximation to a given wavefunction (e.g. ϕ^n). This discretization not only allows to select the spatial step as large as wanted, but it also preserves the very high spatial accuracy, the parallel computing structure and the scalability of the split method developed in [22].

3.2. Time-Splitting Pseudospectral method with PML (TSSP-PML)

As proposed before, we use a splitting of the TDDE into four time-dependent systems (9), (10), (11) and (12). We denote by $\mathbf{x}_h = (x_h, y_h, z_h)$ the nodes of a real-space grid. At iteration n , the approximate wave function is denoted by ψ_h^n . The TSSP (Time-Splitting pseudoSpectral) algorithm then reads

1. **First step:** integration of the generalized transport equation in Fourier space in the x -direction. One sets $\phi_h^n := \Pi_x^T \psi_h^n$, and the system

$$\partial_t \phi + cS_x^{-1}(x)\Lambda_x \partial_x \phi = 0, \quad \phi(t_n, \cdot) = \Pi_x^T \psi(t_n, \cdot),$$

is approximately solved by

$$\phi_h^{n_1} = \phi_h^n - c\Delta t S_x^{-1}(x_h)\Lambda_x [[\partial_x]] \phi_h^n,$$

where $[[\cdot]]$ is defined in (19). We then deduce $\psi_h^{n_1} = \Pi_x \phi_h^{n_1}$. This gives an approximation of Eq. (13), where the corresponding operator is denoted by $\mathcal{P}_h^{(x)}(\Delta t)$.

2. **Second step:** integration of the generalized transport equation in Fourier space in the y -direction

$$\partial_t \phi + cS_y^{-1}(y)\Lambda_y \partial_y \phi = 0.$$

We set $\chi_h^{n_1} := \Pi_y^T \psi_h^{n_1}$ and we approximately solve (14) by using the following scheme

$$\phi_h^{n_2} = \chi_h^{n_1} - c\Delta t S_y^{-1}(y_h)\Lambda_y [[\partial_y]] \chi_h^{n_1}.$$

We then obtain $\psi_h^{n_2} = \Pi_y \phi_h^{n_2}$.

3. **Third step:** setting $\chi_h^{n_2} := \Pi_z^T \psi_h^{n_2}$, we apply the same procedure in the z -direction, and compute $\psi_h^{n_3}$. The corresponding operator is denoted by $\mathcal{P}_h^{(z)}(\Delta t)$.
4. **Fourth step:** integration of the source from t_n to t_{n+1}

$$\begin{aligned} \psi_h^{n+1} &= T \exp \left[-i \int_{t_n}^{t_{n+1}} d\tau [\beta m c^2 - e \boldsymbol{\alpha} \cdot \mathbf{A}_h(\tau)] \right] \\ &\times \exp \left[-ie \int_{t_n}^{t_{n+1}} d\tau V_h(\tau) \right] \psi_h^{n_3}, \end{aligned} \quad (20)$$

where \mathbf{A}_h is the approximate electric potential. The corresponding operator is denoted by $\mathcal{Q}_h^n(\Delta t)$.

This splitting scheme is fully explicit, and can be compactly expressed as a composition of the four operators

$$\psi_h^{n+1} = \mathcal{P}_h^{(x)}(\Delta t) \mathcal{P}_h^{(y)}(\Delta t) \mathcal{P}_h^{(z)}(\Delta t) \mathcal{Q}_h^n(\Delta t) \psi_h^n.$$

In practice, a second-order splitting scheme should be implemented, i.e.

$$\begin{aligned} \psi_h^{n+1} &= \mathcal{P}_h^{(x)}\left(\frac{\Delta t}{4}\right) \mathcal{P}_h^{(y)}\left(\frac{\Delta t}{2}\right) \mathcal{P}_h^{(x)}\left(\frac{\Delta t}{4}\right) \mathcal{P}_h^{(z)}\left(\frac{\Delta t}{2}\right) \mathcal{Q}_h^n(\Delta t) \\ &\mathcal{P}_h^{(z)}\left(\frac{\Delta t}{2}\right) \mathcal{P}_h^{(x)}\left(\frac{\Delta t}{4}\right) \mathcal{P}_h^{(y)}\left(\frac{\Delta t}{2}\right) \mathcal{P}_h^{(x)}\left(\frac{\Delta t}{4}\right) \psi_h^n. \end{aligned} \quad (21)$$

Thanks to the operator $[[\partial_\nu]]$, it is possible to implement the real-space approximation of the overall wave function on a bounded domain imposing in particular PMLs, resulting in the TSSP-PML scheme.

4. Numerical simulation

We propose some numerical experiments illustrating the efficiency of the combined method PML-TSSP method with a second-order operator splitting. We are mainly interested in the evolution of wavepacket either subject to a static potential or of an external field. In our simulations, we have used several libraries which are listed below.

4.1. Technical details about the code and parallel computing aspects

The Fourier transforms are performed with the sequential and parallel version 3.3.4 of `fftw`. Standard linear algebra libraries `gsl` (version 1.9) and `blas` were also used. Finally `openMPI` 1.6.3 was used for message passing with non-blocking communication. The code was implemented in `C++` and the compiler is the version 4.7.0 of `gcc`. In the following, the first three one-dimensional tests are realized by using `matlab`. The tests are performed by using a `C++`-code with MPI-library. The method is implemented on the cluster `mammoth-parallel II` from the RQCHP. The total processing power of this machine is 333 400 GFlops, and possesses 39648 cores: 3216 processors AMD Opteron 12 cores at 2.1 GHz, and 88 processors AMD Opteron 12 cores 2.2 GHz. The total memory is 57.6 TB and the computer-networking communications is Infiniband QDR (4 GB/sec). Regarding the communication between processes, by default `mammoth II` will select the closest processors in the same node, then the processors from the nodes in the same topological ring, and finally through different switch-levels. Notice that for a low number of processors, the communication between the processes within the same node is done thanks to a shared memory. The detailed of the Dirac equation solver without PML is presented in detailed in [4], Section 4. Let us recall the main features of the code in 2-d. In the (x, z) coordinates, we proceed by alternating the directions. We first decompose the domain by layers in the z -direction, then

- We successively perform the evolution (FFT) sequentially in the x -direction, and by layer in the z -direction. Each processor manages one layer in z . A perfect scaling for this step is expected as it does not require any transmission from one node to another.
- For all x , we perform the evolution in the z -direction using the parallel FFT (`fftw`). The performance of this step is then fully dependent on the parallelization of the one-dimensional FFT.

Notice that the presence of the PML does not deteriorate the efficiency of the overall method compared to usual FFT-methods. In particular, the computational complexity is simple to established, and is given by C after N_T time iterations

$$C = \mathcal{O}(N_{T_f} N_x N_z \log(N_x N_z)).$$

The scalability and performance of the TSSP method *without* PML is fully studied in [22], where in particular it is shown a good speed-up of this method.

4.2. Numerical experiments

The second-order TSSP-PML method (21) is implemented, where the discrete operators $[[\cdot]]$ given by (19) are used in the directions $\nu = x, z$. We then choose S_ν as follows, for $\nu = x, z$,

$$S_\nu(\nu) = \begin{cases} 1, & |\nu| < L_\nu^*, \\ 1 + e^{i\theta} \sigma(|\nu| - L_\nu), & L_\nu^* \leq |\nu| < L_\nu. \end{cases} \quad (22)$$

Test 1 : wavepacket subject to an external laser field. In this first test, we consider a wavepacket

$$\boldsymbol{\psi}(x, y, z, 0) = \mathcal{N}[1, 0, 0, 0]^T \times \exp\left(-\frac{(x^2 + y^2 + z^2)}{\Delta^2}\right) \exp(ik_x x), \quad (23)$$

subject to an external potential and propagating with a fixed wavenumber $\mathbf{k} = (5, 0)$, and $\Delta = 128$ in (23). The time step is given by $\Delta t = 4.56 \times 10^{-4}$. The physical domain is $\mathcal{D} = [-8, 8]^2$ and is discretized with $N_x \times N_y = 256^2$ grid points. We impose a linearly polarized electric field such that A_x is identically null, and $A_z(t, x, z)$ is defined as follows

$$A_z(t, x, z) = A_0 \cos(\omega x) \exp\left(-\frac{(T_f - t)^2}{2}\right),$$

with $A_0 = 100/137$, $\omega = 100$, a total of 20 cycles and $T_f = 1.824$. As an example, we report in Fig. 1 the electric potential A_z at time $T = 0.456$ and 1.824 and the initial data. In Fig. 2, we compare the evolution of the density $d(T, x, z) = \sum_{i=1}^4 |\psi_i(T, x, z)|^2$ as a function of time, with i) periodic boundary conditions, with PML of ii) type III and iii) type IV, with $\sigma_0 = 10^{-2}$, $\theta = \pi/4$ as well as iv) type V and VI with $\delta_\nu = L_\nu - L_\nu^*$. The snapshots correspond to times $T = 0.456, 1.14, 1.368$ and 1.824, for respectively the time iterations 1000, 2500, 3000 and 4000. The best absorption is obtained with the Type-VI absorbing function, although the results are relatively close with all the absorbing functions. We report in Fig. 3, the maximum of the density (in logscale) as a function of the time iterations for 6 different absorbing functions, showing that they all provide relatively good properties for truncating the computational domain.

Test 2 : 3-nucleus system. In this test, a Gaussian wavepacket centered at $(0, 0)$ Fig. 4 (Left), is injected in a 3-nucleus interaction potential Fig 4 (Middle)

$$V(x, z) = -\frac{Z_A}{\sqrt{(x - x_A)^2 + (z - z_A)^2 + 2}} - \frac{Z_B}{\sqrt{(x - x_B)^2 + (z - z_B)^2 + 2}} - \frac{Z_C}{\sqrt{(x - x_C)^2 + (z - z_C)^2 + 2}} \quad (24)$$

with $Z_A = Z_B = Z_C = 10 \text{a.u.}$, $(x_A, z_A) = (-1, 0)$, $(x_B, z_B) = (1, 0)$ and $(x_C, z_C) = (0, -1)$. The overall computational domain is $\mathcal{D} = [-6, 6]^2$, with $N_x \times N_y = 128^2$ grid points and $\Delta t = 3 \times 10^{-3}$. We report on Fig. 4 (Right) the total density at time $T = 3 \times 10^{-1}$ a.u., i.e. $d(T, x, z)$, for $(x, z) \in \mathcal{D}$, where $d(T, x, z) = \sum_{i=1}^4 |\psi_i(T, x, z)|^2$, setting $\boldsymbol{\psi} = (\psi_1, \psi_2, \psi_3, \psi_4)$ as the Dirac wave function. Without external excitation the wavepacket is then trapped by the potential. We then plug an external laser field which drives the wavepacket: a linearly polarized electric field is imposed such that A_x is identically null, and $A_z(t, x, z)$ is defined as follows

$$A_z(t, x, z) = A_0 \cos(\omega x) \exp\left(-\frac{(T - t)^2}{2}\right),$$

with $A_0 = 1000/137$, $\omega = 1$, and a total of 2 cycles. We report the z -component of the external laser potential in Fig. 5 at final time. We also include a non-null wavenumber in

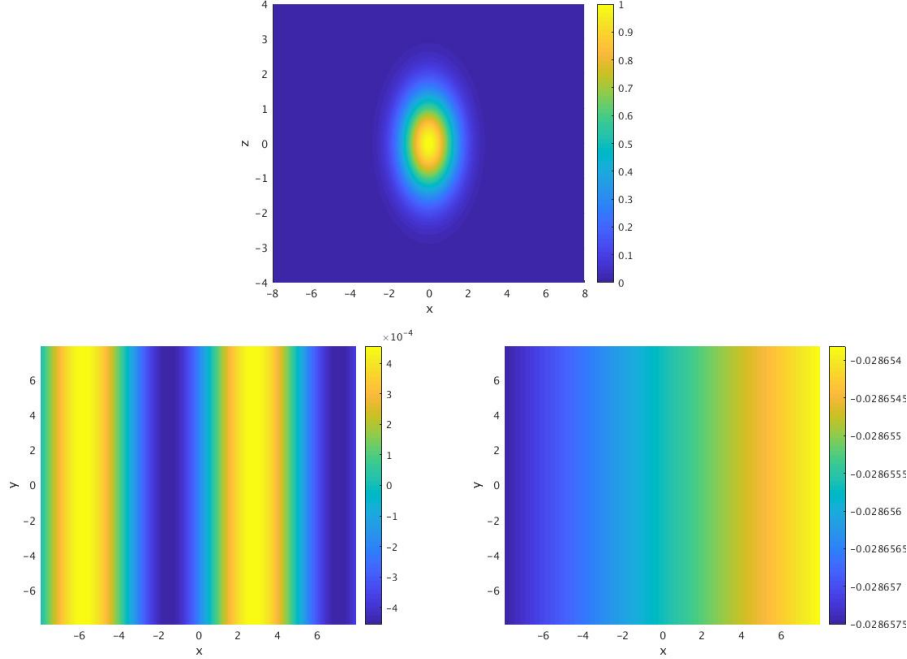


Figure 1: **Test 1** : initial density (top), $A_z(T, x, y)$ at times $T = 0.456$ (Bottom left) and 1.824 (Bottom right).

the initial wavepacket, $\mathbf{k} = (10, 0)$, out of the ions influence. The wavepacket will eventually be absorbed by the PML unlike the solution without PML.

At times $t = 3 \times 10^{-2}$, $t = 6 \times 10^{-2}$ a.u., $t = 3 \times 10^{-1}$ and $t = 3.6 \times 10^{-1}$, we compare 3 solutions: 1) the solution of reference computed on $[-18, 18] \times [-18, 18]$, 2) the solution without PML, and 3) the solution with Type V-PML and $\sigma_0 = 10^{-2}$, $\theta = \pi/4$, and $\delta = 1.2$. At time $t = 6 \times 10^{-2}$, the 3 solutions look identical, as the wavefunction has not reached the boundary of the computational domain $[-6, 6] \times [-6, 6]$. At $t = T = 3 \times 10^{-1}$, we however clearly see that the wavefunction of reference has mainly leaved the region $[-6, 6] \times [-6, 6]$, while the PML solution was almost totally absorbed and the solution without PML, was maintained in the computational domain due to non-absorbing boundary layers. This is also illustrated on Fig. 7, where the ℓ^2 -norm as function of time in the \mathcal{D} is represented for the 3 solutions. We see that, unlike the solution without PML, the PML-solution makes decrease the ℓ^2 - norm, thanks to the absorbing layers. We also report in Fig. 7 (Left), we represent the solution of reference at time $T = 0.3$ a.u. in a bigger domain $[-18, 18] \times [-18, 18]$. By comparison, we see that on this example, the solution of reference has also a decreasing ℓ^2 - norm in the zone \mathcal{D} ($(t, \|d_{\mathcal{D}}^{\text{Ref}}(t, \cdot)\|_2)$), see Fig. 7 where the ℓ^2 -norm is represented in logscale as a function of time (Right). We also report the solution of reference in the domain $[-18, 18] \times [-18, 18]$ at time $T = 0.36$ a.u.

Test 3 : evolution of wavepacket subject to a repulsive weakly nonlinear poten-

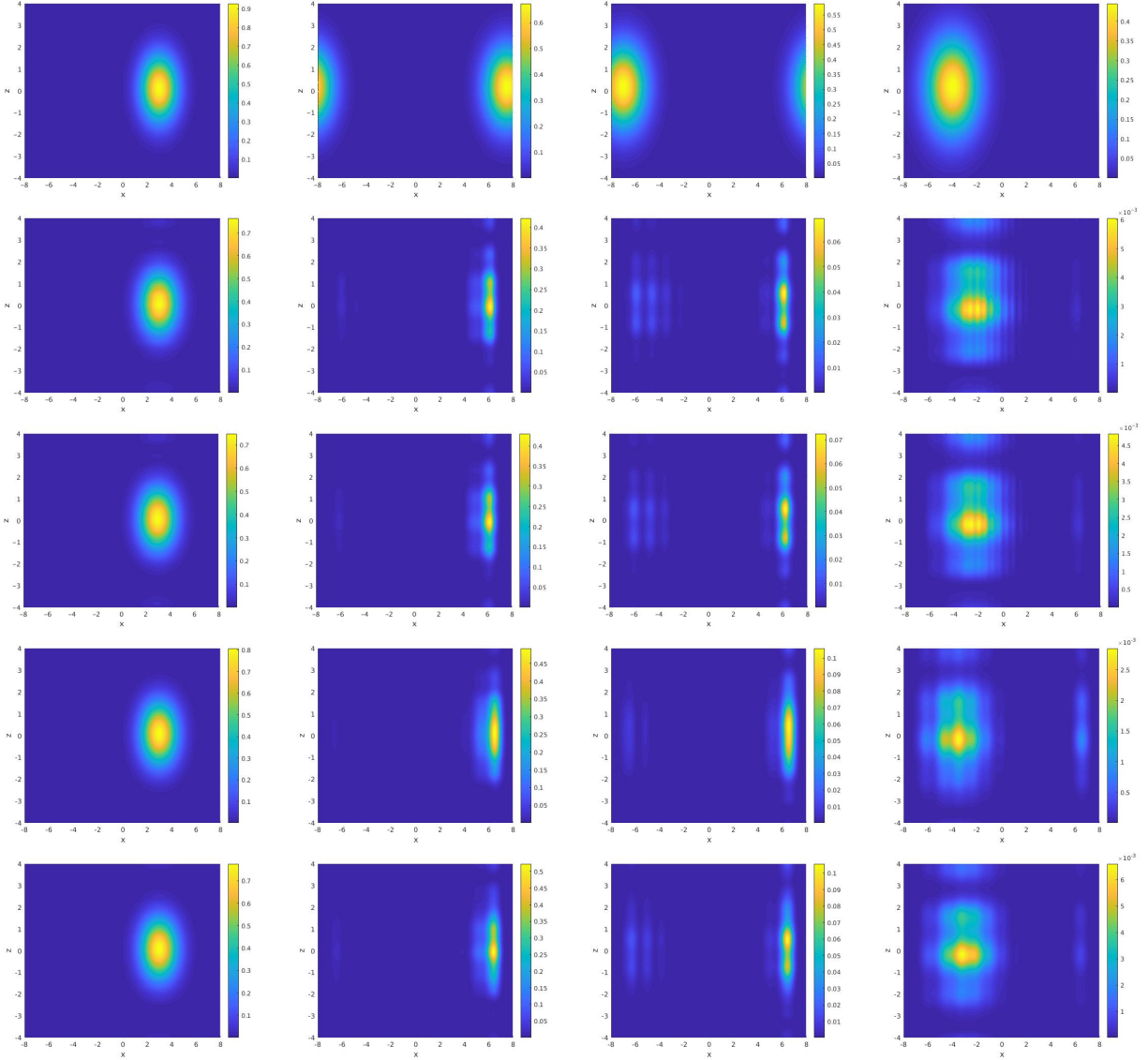


Figure 2: **Test 1** : density at times $T = 0.456, 1.14, 1.368$ and 1.824 (first line) with periodic boundary conditions (without PML). The second (respectively third) line reports the results for the density with TSSP-PML, with a PML of Type-III (respectively Type-IV), setting $\sigma_0 = 10^{-2}$, $\theta = \pi/4$. The fourth (respectively fifth) line gives the same kind of results but for the Type-V (respectively Type-VI) PML, with $\sigma_0 = 10^{-2}$, $\theta = \pi/4$ and $\delta_\nu = L_\nu - L_\nu^*$.

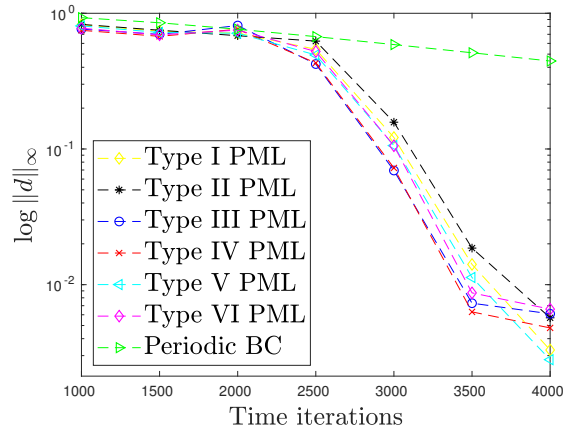


Figure 3: **Test 1** : maximum of the density in logscale, as a function of the time iteration, for 6 different types of PML.

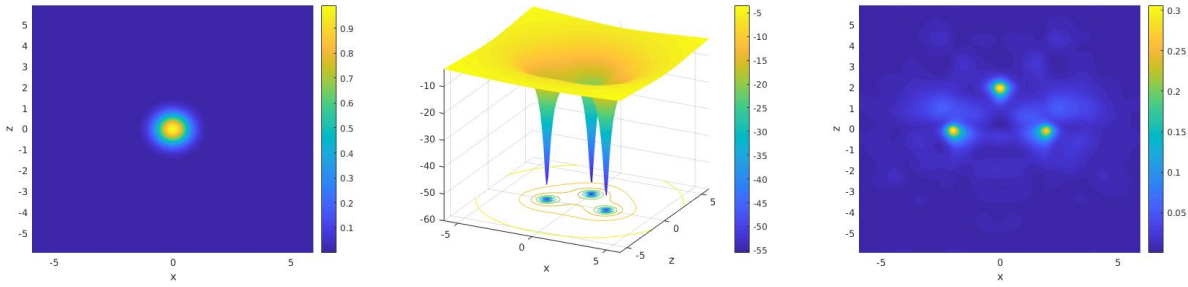


Figure 4: **Test 2** : (Left) Initial density. (Middle) 3-nucleus potential. (Right) Density at time $T = 3 \times 10^{-1}$ a.u. without external laser field.

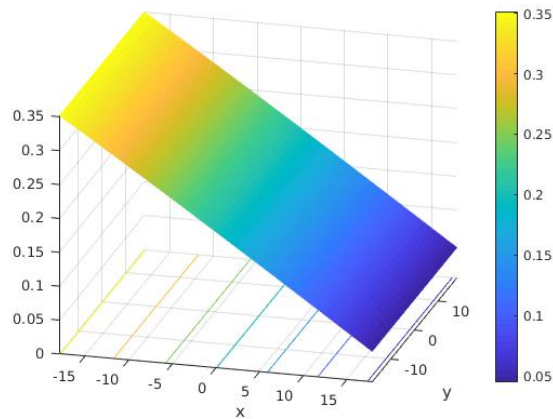


Figure 5: **Test 2** : z -component of the external laser potential: $A_z(T, x, z)$ for $T = 3 \times 10^{-1}$ a.u.

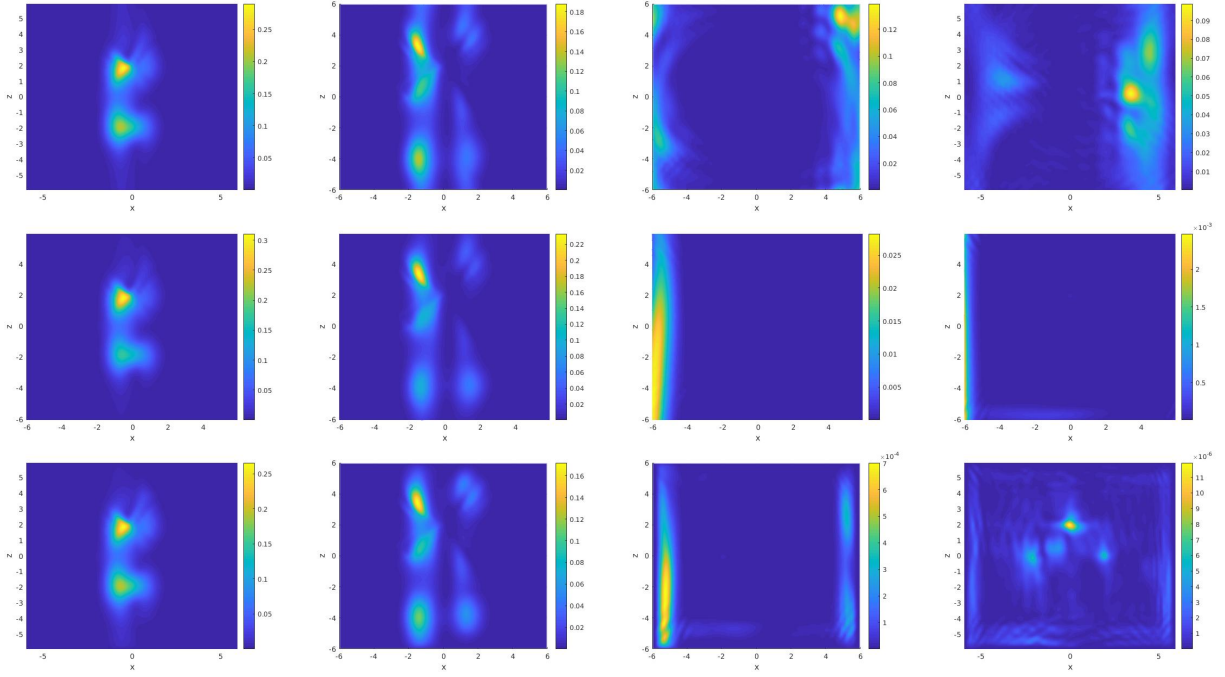


Figure 6: **Test 2** : From top to bottom: No PML, reference and Type V-PML solutions at time $t = 3 \times 10^{-2} a.u.$, $t = 6 \times 10^{-2} a.u.$, $t = 3 \times 10^{-1} a.u.$ and $t = 3.6 \times 10^{-1} a.u.$,

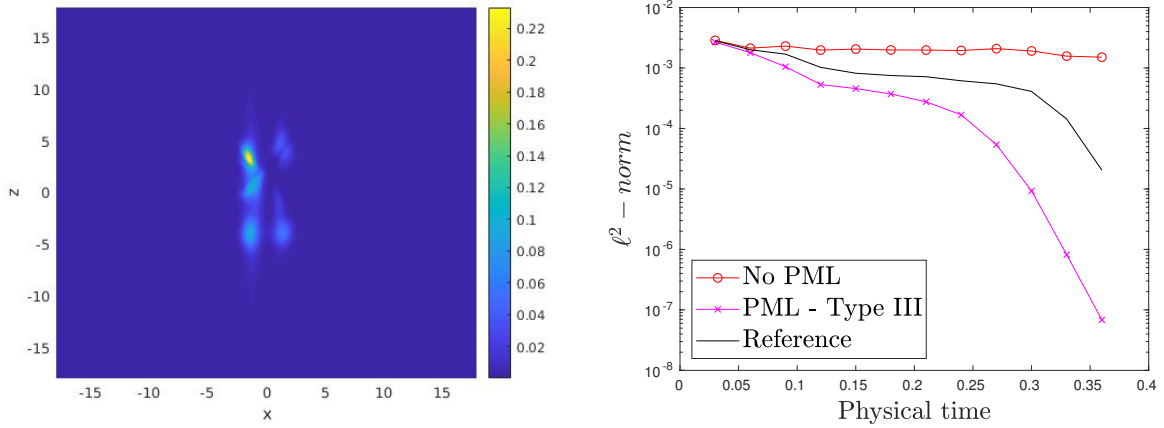


Figure 7: **Test 2** : (Left) Solution of reference at time $T = 6 \times 10^{-2} a.u.$ in the domain $[-18, 18] \times [-18, 18]$. (Right) ℓ^2 -norm in logscale of the 3 solutions (No PML, Reference, Type V-PML) as a function of time in \mathcal{D} .

tial. We consider the two-dimensional Dirac equation with a nonlinear potential

$$V(x, z, \psi) = \frac{Z_A}{\sqrt{(x - x_A)^2 + (z - z_A)^2 + 1}} + \frac{Z_B}{\sqrt{(x - x_B)^2 + (z - z_B)^2 + 1}} + |\psi|^2, \quad (25)$$

with $Z_A = Z_B = 2$, $(x_A, z_A) = (-1, 4)$ and $(x_B, z_B) = (1, 4)$. Notice that the sign of the potential makes it repulsive. The initial density with wave vector $\mathbf{k} = (2, 10)$ is represented in Fig. 8. More specifically, the initial data is given by

$$\psi(x, y, z, 0) = \mathcal{N}[1, 0, 0, 0]^T \times \exp\left(-\frac{x^2 + y^2 + z^2}{\Delta^2}\right) \exp(\mathbf{i}k_x x), \quad (26)$$

where $\Delta = 128$ in (26) and \mathcal{N} is a normalization coefficient, such that $\|\psi(\cdot, 0)\|_{(L^2(\mathcal{D}))^4} = 1$. The overall computational domain is $\mathcal{D} = [-8, 8]^2$, with $N_x \times N_y = 256^2$ grid points and $\Delta t = 4.56 \times 10^{-4}$. We report on Fig. 9 the total density at time $T = 0.912$ a.u. in logscale, i.e. $\log(d(T, x, z))$, for $(x, z) \in \mathcal{D}$, where $d(T, x, z) = \sum_{i=1}^4 |\psi_i(T, x, z)|^2$, setting $\psi = (\psi_1, \psi_2, \psi_3, \psi_4)$ as the Dirac wave function. The nonlinearity is numerically treated explicitly. The use of the logscale allows to fairly report the accuracy of the PML. In (22), we take $L_\nu = 8$, $L_\nu^* = 0.8L_\nu$, $\theta = \pi/4$ (similarly to the Schrödinger equation [3, 52]), and we pick the Type-IV PML, i.e. $\sigma : \nu \mapsto \sigma_0/\nu^2$ (singular profile [3]). We represent the solution with different values of σ_0 . These results show that the PML properly absorbs except for $\sigma_0 = 5$, with reflection magnitude as weak as 10^{-6} for $\sigma_0 = 10^{-2}$. Let us remark that other PMLs could be considered as well [43], but we intend here to prove the feasibility of the method for various PMLs. For completeness and by comparisons with results obtained in Fig. 9, we also report in Fig. 10 the solution to the Dirac equation in \mathcal{D} with zero Dirichlet boundary condition by using the real-space quantum lattice Boltzmann method proposed in [22] and illustrating the total wave reflection at the domain boundary when PMLs or ABCs are not used. This simple example illustrates the fact without using PML and or even low-order ABC a wavefunction is totally reflected. This is a standard issue when solving the Dirac equation, in particular when studying laser-molecule interaction. We report in Fig. 11 (left), the maximum of the density as a function of time for $\sigma_0 = 10^{-3}, 10^{-2}, 10^{-1}, 1, 5$ in logscale, with the PML of Type IV for $\theta = \pi/4$. We clearly see that $\sigma_0 = 10^{-2}$ provides the best absorption properties. We next compare in Fig. 12, for $\sigma_0 = 10^{-2}$, the reflection for $\theta = \pi/16, \theta = \pi/8, \theta = \pi/4$ and $\theta = \pi/2$ showing the importance of properly selecting θ , with best absorption at $\theta = \pi/16$. We report in Fig. 11 (right), the maximum of the density as a function of the time iteration for different values of $\theta = \pi/16, \pi/8, \pi/4, \pi/2$ with Type IV-PML. We again see an optimal performance with $\theta = \pi/16$ but $\theta = \pi/8$ or $\theta = \pi/4$ also provides some good results, meaning that the PML is relatively stable with θ . In the last test, we compare in Fig. 13, the efficiency of the PML for four different absorbing functions (Types I to IV), with respectively $\sigma(\nu) = \sigma_0(\nu + \delta_\nu)^2$, $\sigma(\nu) = \sigma_0(\nu + \delta_\nu)^3$, $\sigma(\nu) = -\sigma_0/\nu$ and $\sigma(\nu) = \sigma_0/\nu^2$. We see that the best results are obtained for the Type-IV PML, a similar quality being also obtained for the Types V and VI PMLs (not reported here).

These tests clearly show the relevance of the combination of the TSSP method with PMLs, as we simultaneously benefit from the efficiency and accuracy of FFTs and the high absorption feature of PMLs to avoid reflections at the boundary.

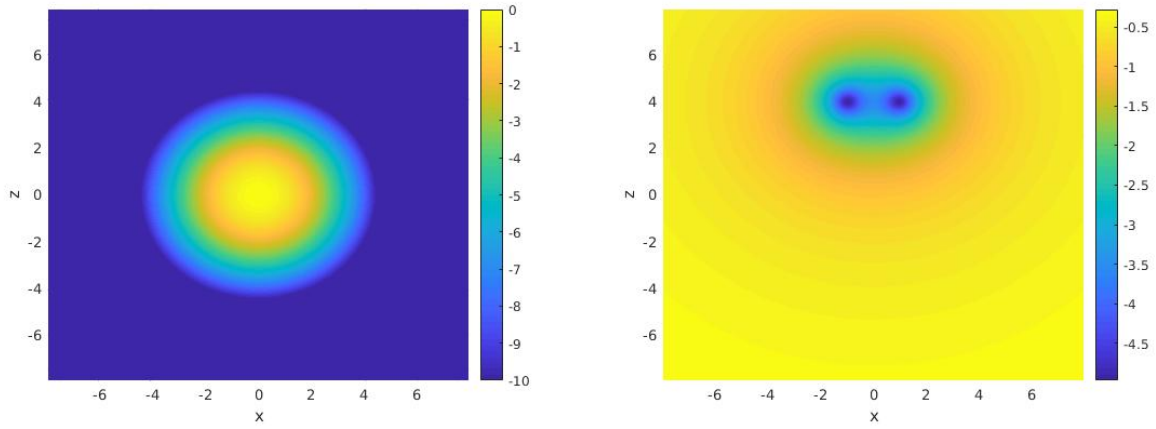


Figure 8: **Test 3** : initial density in logscale (Left) and static potential (Right).

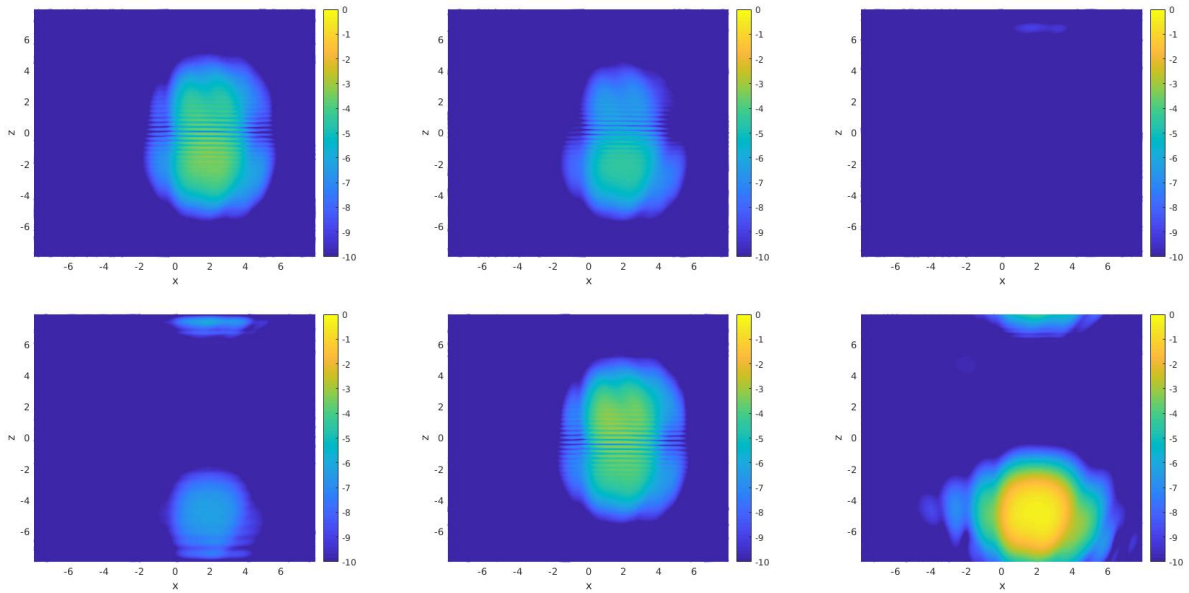


Figure 9: **Test 3** : logarithm of the density at time $T = 0.912$ (from top-left to bottom-right) for the PML with parameters $\sigma_0 = 1$, $\sigma_0 = 10^{-1}$, $\sigma_0 = 10^{-2}$, $\sigma_0 = 10^{-3}$, $\sigma_0 = 5$, and finally for a periodic boundary condition ($S = 1$).

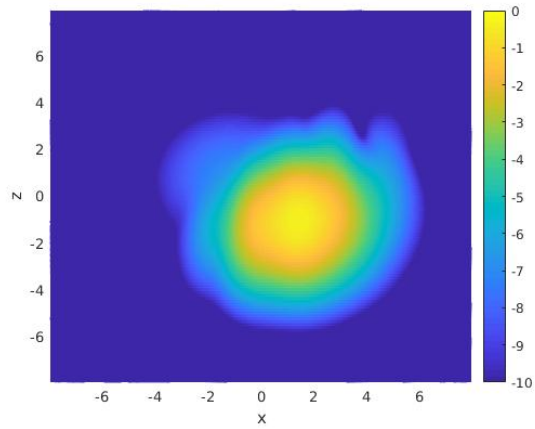


Figure 10: **Test 3** : logarithm of the density at time $T = 0.912$ with null Dirichlet boundary condition. This test illustrates that artificial wave-reflecting occurs with real space methods (here a quantum lattice Boltzmann method [22]) are implemented without PML or ABC.

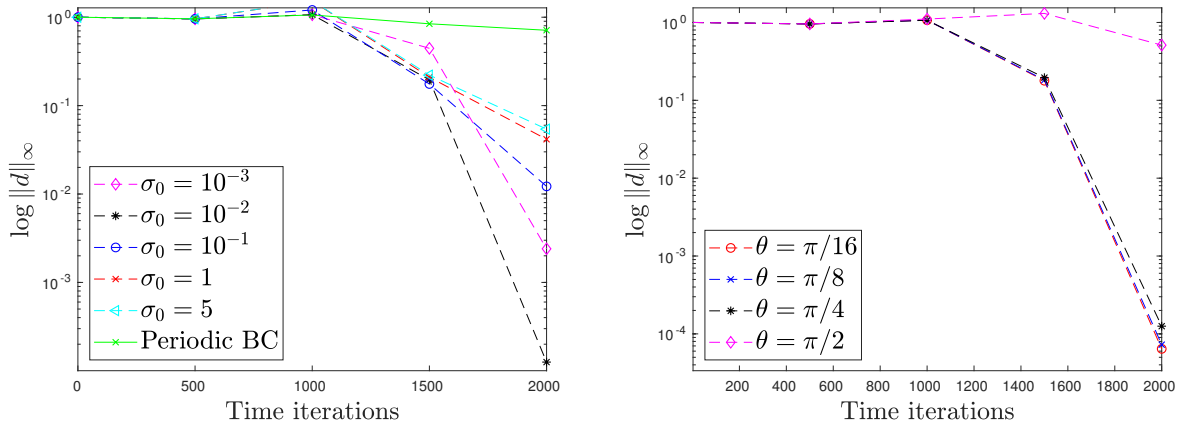


Figure 11: **Test 3** : PML of type IV (Left) maximum of the density as a function of the time iteration with 5 different values of σ and for $\theta = \pi/4$; (Right) maximum of the density as a function of the time iteration for $\theta = \pi/16, \pi/8, \pi/4, \pi/2$ and $\sigma_0 = 10^{-2}$.

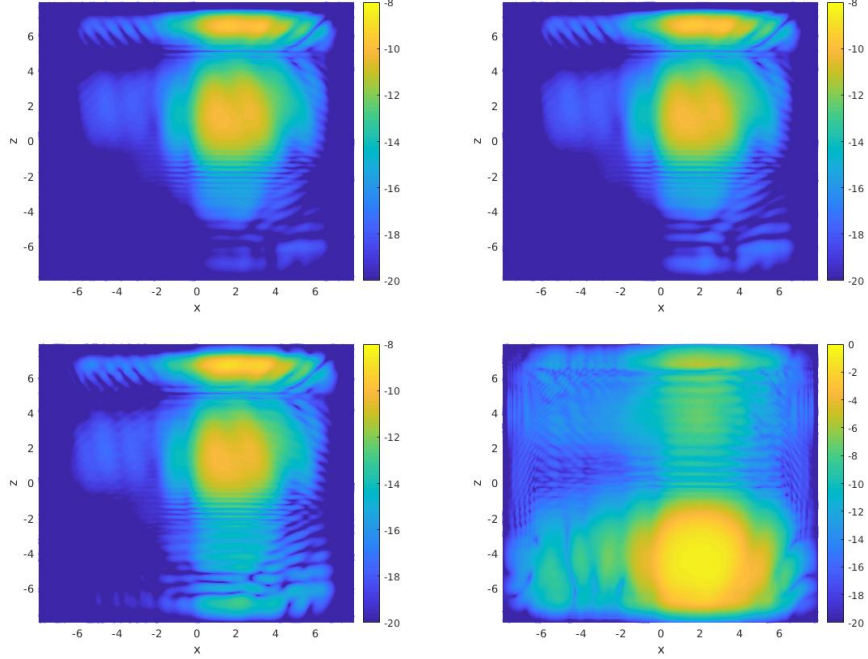


Figure 12: **Test 3** : logarithm of the density at time $T = 0.912$ for $\sigma_0 = 10^{-2}$ and $\theta = \pi/16$, $\theta = \pi/8$, $\theta = \pi/4$ and $\theta = \pi/2$.

Test 4 : convergence. In this last test, we propose a simple convergence benchmark. A wavepacket with wavenumber $\mathbf{k} = (5, 0)$ is propagating in vacuum without external electric field. We plot the initial density, and final solution with periodic solution on $\mathcal{D} = [-8, 8]^2$ in Fig. 14 (Left, Middle). We report the supremum of the solution for $N_x = N_y = 32, 256, 320, 512, 640, 768$ with the PML of Type-III, for $\sigma_0 = 10^{-2}$, $\theta = \pi/4$, fixing the time step to $\Delta t = 1.8 \times 10^{-3}$. We report the maximum of the density at final time T in logscale with the different meshes

$$\left\{ (x, y, \ln \sup |d(T, x, z)|) : (x, z) \in [-8, 8]^2 \right\}.$$

Moreover in Fig. 14 (Right), we observe an exponential convergence up to a certain precision. Notice that what is reported is not the comparison with a solution of reference, but the maximum of the solution over the physical domain, including the PML. In other words the smaller the maximum, the better the absorption. The saturation error comes from the limit of the PML accuracy and error in time (second-order splitting). This again shows the high accuracy of the TSSP with PML.

5. Conclusion

In this paper, we have proposed a simple time-splitting pseudospectral method which allows for the numerical computation of IBVP for the Dirac equation with non-reflecting

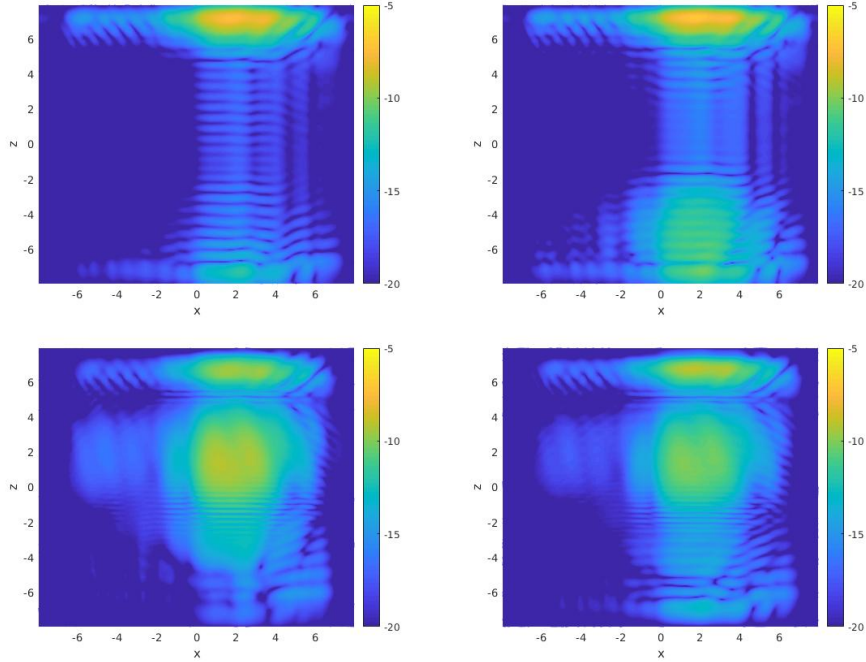


Figure 13: **Test 3** : logarithm of the density at time $T = 0.912$ for $\sigma_0 = 10^{-2}$, $\theta = \pi/4$, $\delta_\nu = L_\nu - L_\nu^*$, and absorption function σ of types I to IV.

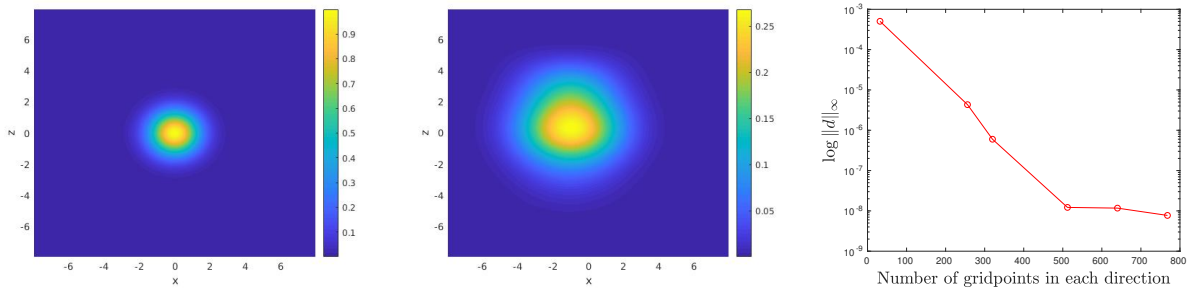


Figure 14: **Test 3** : initial data (Left), periodic boundary conditions (Middle), convergence with the Type-III PML (Right), for $\sigma_0 = 10^{-2}$, $\theta = \pi/4$ and $N_x = N_y = 32, 256, 320, 512, 640, 768$.

PML. Some numerical experiments have shown that the method preserves the accuracy of the PML with static or time-dependent external potentials. Different absorbing functions were considered and tested. The implementation strategy is developed for the TSSP approximation, but can be directly extended to other numerical schemes including implicit. We think that Fourier-based codes solving the time-dependent Dirac equation can easily be adapted to include the absorbing layers, hence drastically reducing the negative effect of periodic conditions and simultaneously avoiding artificial wave reflections. We next plan to analyze mathematically the stability and convergence of the method as well as the PML accuracy for different types of absorbing functions.

Acknowledgments. X. ANTOINE was partially supported by the French National Research Agency project NABUCO, grant ANR-17-CE40-0025. E. LORIN received support from NSERC through the Discovery Grant program.

References.

- [1] X. Antoine, A. Arnold, C. Besse, M. Ehrhardt, and A. Schaedle. A review of transparent and artificial boundary conditions techniques for linear and nonlinear Schroedinger equation. *Commun. Comput. Phys.*, 4(4):729–796, 2008.
- [2] X. Antoine, C. Besse, and V. Rispoli. High-order IMEX-spectral schemes for computing the dynamics of systems of nonlinear Schrödinger/GrossPitaevskii equations. *J. Comput. Phys.*, 327:252–269, 2016.
- [3] X. Antoine, C. Geuzaine, and Q. Tang. Perfectly Matched Layer for computing the dynamics of nonlinear Schrödinger equations by pseudospectral methods. Application to rotating Bose-Einstein condensates. *In preparation*, 2018.
- [4] X. Antoine and E. Lorin. Computational performance of simple and efficient sequential and parallel Dirac equation solvers. *Comput. Phys. Commun.*, 220:150–172, 2017.
- [5] X. Antoine, E. Lorin, J. Sater, F. Fillion-Gourdeau, and A.D. Bandrauk. Absorbing boundary conditions for relativistic quantum mechanics equations. *J. Comput. Phys.*, 277:268–304, 2014.
- [6] X. Antoine, E. Lorin, and Q. Tang. A friendly review of absorbing boundary conditions and perfectly matched layers for classical and relativistic quantum waves equations. *Molecular Physics*, 115(15-16):1861–1879, 2017.
- [7] W. Bao, Y. Cai, X. Jia, and Q. Tang. Numerical methods and comparison for the Dirac equation in the nonrelativistic limit regime. *J. Sc. Comput.*, 71(3):1–41, 2017.
- [8] W. Bao and X.-G. Li. An efficient and stable numerical method for the Maxwell-Dirac system. *J. Comput. Phys.*, 199(2):663–687, 2004.

- [9] H. Bauke and C.H. Keitel. Accelerating the Fourier split operator method via graphics processing units. *Comput. Phys. Commun.*, 182(12):2454–2463, 2011.
- [10] U. Becker, N. Grun, and W. Scheid. Solution of the time-dependent Dirac equation by the finite difference method and application for $\text{Ca}^{20+} + \text{U}^{91+}$. *J. of Phys. B: Atomic and Molecular Physics*, 16(11):1967, 1983.
- [11] R. Beerwerth and H. Bauke. Krylov subspace methods for the Dirac equation. *Comput. Phys. Commun.*, 188:189 – 197, 2015.
- [12] A. Bermúdez, L. Hervella-Nieto, A. Prieto, and R. Rodríguez. An exact bounded perfectly matched layer for time-harmonic scattering problems. *SIAM J. Sci. Comput.*, 30:312–338, 2007.
- [13] A. Bermúdez, L. Hervella-Nieto, A. Prieto, and R. Rodríguez. An optimal perfectly matched layer with unbounded absorbing function for time-harmonic acoustic scattering problems. *J. Comput. Phys.*, 223:469–488, 2007.
- [14] J. W. Braun, Q. Su, and R. Grobe. Numerical approach to solve the time-dependent Dirac equation. *Phys. Rev. A*, 59(1):604–612, Jan 1999.
- [15] W.C. Chew and Q.H. Liu. Perfectly matched layers for elastodynamics: A new absorbing boundary condition. *J. Comput. Acoustics*, 4(4):341–359, 1996.
- [16] F. Collino and P. Monk. The perfectly matched layer in curvilinear coordinates. *SIAM J. Sci. Comput.*, 19:2061–2090, 1998.
- [17] T. Colonius. Modeling artificial boundary conditions for compressible flow. *Annual Review of Fluid Mechanics*, 36:315–345, 2004.
- [18] F. H. M. Faisal. A four-component Dirac theory of ionization of a Hydrogen molecular ion in a super-intense laser field. *J. Phys. B: At. Mol. Opt. Phys.*, 42(171003), 2009.
- [19] C. Farrell and U. Leonhardt. The perfectly matched layer in numerical simulations of nonlinear and matter waves. *Journal of Optics B-Quantum and Semiclassical Optics*, 7(1):1–4, 2005.
- [20] F. Fillion-Gourdeau, P. Blain, D. Gagnon, C. Lefebvre, and S. Maclean. Numerical computation of dynamical schwinger-like pair production in graphene. *Russian Physics Journal*, 59(11):1875–1880, 2017.
- [21] F. Fillion-Gourdeau, D. Gagnon, C. Lefebvre, and S. Maclean. Time-domain quantum interference in graphene. *Physical Review B*, 94(12), 2016.
- [22] F. Fillion-Gourdeau, E. Lorin, and A. D. Bandrauk. Numerical solution of the time-dependent Dirac equation in coordinate space without fermion-doubling. *Comput. Phys. Commun.*, 183(7):1403 – 1415, 2012.

- [23] F. Fillion-Gourdeau, E. Lorin, and A.D. Bandrauk. Numerical solution of the time-independent Dirac equation for diatomic molecules: B-splines without spurious states. *Phys. Rev. A - Atomic, Molecular, and Optical Physics*, 85(2), 2012.
- [24] F. Fillion-Gourdeau, E. Lorin, and A.D. Bandrauk. Enhanced schwinger pair production in many-centre systems. *Journal of Physics B: Atomic, Molecular and Optical Physics*, 46(17), 2013.
- [25] F. Fillion-Gourdeau, E. Lorin, and A.D. Bandrauk. Resonantly enhanced pair production in a simple diatomic model. *Phys. Rev. Lett.*, 110(1), 2013.
- [26] F. Fillion-Gourdeau, E. Lorin, and A.D. Bandrauk. A split-step numerical method for the time-dependent Dirac equation in 3-d axisymmetric geometry. *J. Comput. Phys.*, 272:559–587, 2014.
- [27] F. Fillion-Gourdeau, E. Lorin, and A.D. Bandrauk. Galerkin method for unsplit 3-d Dirac equation using atomically/kinetically balanced B-spline basis. *J. Comput. Phys.*, 307:122–145, 2016.
- [28] C. Fischer and O. Zatsarinny. A B-spline Galerkin method for the Dirac equation. *Comput. Phys. Commun.*, 180(6):879 – 886, 2009.
- [29] F. Gelis, K. Kajantie, and T. Lappi. Quark-antiquark production from classical fields in heavy-ion collisions: 1 + 1 dimensions. *Phys. Rev. C*, 71(2):024904, Feb 2005.
- [30] A. Gonoskov, I. Gonoskov, C. Harvey, A. Ilderton, A. Kim, M. Marklund, G. Mourou, and A. Sergeev. Probing nonperturbative QED with optimally focused laser pulses. *Phys. Rev. Lett.*, 111:060404, Aug 2013.
- [31] I. P. Grant. B-spline methods for radial Dirac equations. *J. of Phys. B: Atomic, Molecular and Optical Physics*, 42(5):055002, 2009.
- [32] B.-Y. Guo, J. Shen, and C.-L. Xu. Spectral and pseudospectral approximations using Hermite functions: Application to the Dirac equation. *Advances in Computational Mathematics*, 19(1-3):35–55, 2003.
- [33] R. Hammer, W. Ptz, and A. Arnold. A dispersion and norm preserving finite difference scheme with transparent boundary conditions for the Dirac equation in (1+1)d. *J. Comput. Phys.*, 256:728–747, 2014.
- [34] F.Q. Hu. On absorbing boundary conditions for linearized Euler equations by a perfectly matched layer. *J. Comput. Phys.*, 129(1):201–219, 1996.
- [35] F.Q. Hu. A stable, perfectly matched layer for linearized Euler equations in unsplit physical variables. *J. Comput. Phys.*, 173(2):455–480, 2001.
- [36] C. Itzykson and J. B. Zuber. *Quantum Field Theory*. McGraw-Hill, 1980.

- [37] M. I. Katsnelson, K. S. Novoselov, and A. K. Geim. Chiral tunnelling and the Klein paradox in graphene. *Nature Physics*, 2:620 – 625, 2006.
- [38] O. Kullie, C. Dusterhoft, and D. Kolb. Dirac-Fock finite element method (FEM) calculations for some diatomic molecules. *Chemical Physics Letters*, 314(3-4):307 – 310, 1999.
- [39] E. Lorin and A. Bandrauk. A simple and accurate mixed P_0 - Q_1 solver for the Maxwell-Dirac equations. *Nonlin. Anal. Real World Appl.*, 12(1):190–202, 2011.
- [40] G. R. Mocken and C. H. Keitel. Quantum dynamics of relativistic electrons. *J. Comput. Phys.*, 199(2):558 – 588, 2004.
- [41] G. R. Mocken and C. H. Keitel. FFT-split-operator code for solving the Dirac equation in 2+1 dimensions. *Comput. Phys. Commun.*, 178(11):868 – 882, 2008.
- [42] A. Nissenand and G. Kreiss. An optimized perfectly matched layer for the Schroedinger equations. *Commun. Comput. Phys.*, 9(1):147–179, 2011.
- [43] O. Pinaud. Absorbing layers for the Dirac equation. *J. Comput. Phys.*, 289:169–180, 2015.
- [44] J. Reinhardt, B. Müller, and W. Greiner. Theory of positron production in heavy-ion collisions. *Phys. Rev. A*, 24:103–128, Jul 1981.
- [45] Y. Salamin, S. X. Hu, K. Z. Hatsagortsyan, and C. H. Keitel. Relativistic high-power laser-matter interactions. *Physics Reports*, 427(2-3):41 – 155, 2006.
- [46] S. Selstø, E. Lindroth, and J. Bengtsson. Solution of the Dirac equation for hydrogenlike systems exposed to intense electromagnetic pulses. *Phys. Rev. A*, 79(4):043418, Apr 2009.
- [47] M.E. Taylor. *Pseudodifferential Operators*. Princeton University Press, Princeton, NJ, 1981.
- [48] S.V. Tsynkov. Numerical solution of problems on unbounded domains. a review. *Applied Numerical Mathematics*, 27(4):465–532, 1998.
- [49] E. Turkel and A. Yefet. Absorbing PML boundary layers for wave-like equations. *Applied Numerical Mathematics*, 27(4):533–557, 1998.
- [50] J. C. Wells, B. Segev, and J. Eichler. Asymptotic channels and gauge transformations of the time-dependent Dirac equation for extremely relativistic heavy-ion collisions. *Phys. Rev. A*, 59(1):346–357, Jan 1999.
- [51] Y.Q. Zeng, J.Q. He, and Q.H. Liu. The application of the perfectly matched layer in numerical modeling of wave propagation in poroelastic media. *Geophysics*, 66(4):1258–1266, 2001.

- [52] C. Zheng. A perfectly matched layer approach to the nonlinear Schrödinger wave equation. *J. Comput. Phys.*, 227:537–556, 2007.